UNIVERSITYOF BIRMINGHAM

Influence of spin-orbit effects on structures and dielectric properties of neutral lead clusters

Götz, D. A.; Shayeghi, A.; Johnston, R. L.; Schwerdtfeger, P.; Schäfer, R.

[Link to publication on Research at Birmingham portal](#)

Influence of spin-orbit effects on structures and dielectric properties of neutral lead clusters

D. A. Götz, A. Shayeghi, R. L. Johnston, P. Schwerdtfeger, and R. Schäfer

---

Articles you may be interested in

Strong spin–orbit effects in small Pt clusters: Geometric structure, magnetic isomers and anisotropy
J. Chem. Phys. **134**, 034107 (2011); 10.1063/1.3530799

The role of dimensionality on the quenching of spin-orbit effects in the optics of gold nanostructures
J. Chem. Phys. **129**, 144110 (2008); 10.1063/1.2990745

Evolution of the electronic structure of Be clusters
J. Chem. Phys. **123**, 074329 (2005); 10.1063/1.2001655

Infrared vibronic absorption spectrum and spin–orbit calculations of the upper spin–orbit component of the Au 3 ground state
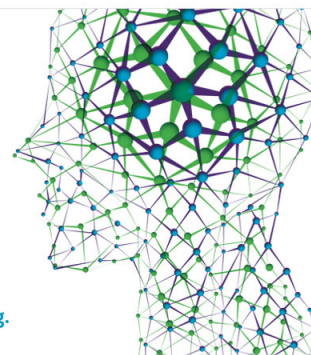J. Chem. Phys. **117**, 1614 (2002); 10.1063/1.1487815

Study of relativistic effects on nuclear shieldings using density-functional theory and spin–orbit pseudopotentials
J. Chem. Phys. **114**, 61 (2001); 10.1063/1.1330208

Influence of spin-orbit effects on structures and dielectric properties of neutral lead clusters

D. A. Götz,[1,a)] A. Shayeghi,[1] R. L. Johnston,[2] P. Schwerdtfeger,[3] and R. Schäfer[1]

[1]*Eduard-Zintl-Institut für Anorganische und Physikalische Chemie, Technische Universität Darmstadt, 64287 Darmstadt, Germany*
[2]*School of Chemistry, University of Birmingham, Edgbaston, Birmingham B15 2TT, United Kingdom*
[3]*Centre for Theoretical Chemistry and Physics, The New Zealand Institute for Advanced Study, Massey University (Albany), Bob Tindall Bldg., 0745 Auckland, New Zealand*

Combining molecular beam electric deflection experiments and global optimization techniques has proven to be a powerful tool for resolving equilibrium structures of neutral metal and semiconductor clusters. Herein, we present electric molecular beam deflection experiments on Pb_N ($N = 7–18$) clusters. Promising structures are generated using the unbiased Birmingham Cluster Genetic Algorithm approach based on density functional theory. The structures are further relaxed within the framework of two-component density functional theory taking scalar relativistic and spin orbit effects into account. Quantum chemical results are used to model electric molecular beam deflection profiles based on molecular dynamics calculations. Comparison of measured and simulated beam profiles allows the assignment of equilibrium structures for the most cluster sizes in the examined range for the first time. Neutral lead clusters adopt mainly spherical geometries and resemble the structures of lead cluster cations apart from Pb_{10}. Their growth pattern deviates strongly from the one observed for tin and germanium clusters. © 2014 AIP Publishing LLC. [http://dx.doi.org/10.1063/1.4872369]

I. INTRODUCTION

The chemistry and physics of lead is strongly influenced by scalar relativistic (SR) and spin-orbit (SO) coupling effects,[1] the latter gives rise to a splitting of the *p*-shell into a lower lying $p_{1/2}$ and a doubly degenerate $p_{3/2}$; this splitting is 1.50 eV for the lead atom.[2] These strong relativistic effects entail distinct features in the chemistry of lead compounds, e.g., the preference of +II over +IV oxidation states (inert pair effect),[3] and the low stability of lead compounds.[4,5] This is manifested impressively in the standard voltage of the lead acid battery as pointed out by Pyykkö and co-workers.[6] The importance of relativistic effects on bulk properties of lead was recognized as early as 1965.[7,8] Hermann *et al.*[9] later attributed the preference for fcc structures in contrast to diamond-like structures and the reduced cohesive energy to SO effects. Closed $p_{1/2}$ subshell effects become even more pronounced for the heavier homolog flevorium, which is predicted to exhibit almost rare-gas like properties.[10,11]

SO coupling effects on lead clusters with six or less atoms were carefully examined by Armbruster *et al.*[12] using a two-component (2c) density functional theory (DFT) implementation. Degeneracies leading to Jahn-Teller distortions at the SR level of theory are lifted if SO effects are included. Pb_6 is D_{4h} symmetric at the SR level of theory but becomes octahedral if SO effects are taken into account. The weakening of the Pb–Pb bond also leads to elongated bond distances and lower cohesive energies as observed for the bulk.[9]

Lead cluster ions have been subject to numerous studies, for example, surface induced dissociation experiments,[13] ion mobility,[14,15] and collision induced dissociation measurements.[15] These experiments mainly suggest spherical cluster geometries up to 32 atoms. Photoelectron spectroscopy indicates the onset of a semi-conductor to metal transition for lead anions at about 20 atoms.[16–18]

Despite the comprehensive work on lead cluster ions, experimental studies on neutral species are rare at present. A few theoretical studies were dedicated to them.[19] Wang *et al.*[20] studied neutral lead clusters up to 22 atoms by SR-DFT and found mainly layered stacking structures for Pb_N ($N \leq 14$). Rajesh and Majumder[21] reported several isomers for cluster sizes with up to 15 atoms using initial geometries from Si, Ge, and Sn clusters, relative energies determined based on SO-DFT single point calculations. Li *et al.*[22] employed a tight-binding genetic algorithm (GA) approach followed by SR-DFT optimizations and SO single point calculations. They noted the deviation of Pb_N structures from the motifs found for tin and germanium for $N \leq 7$. Lei *et al.*[23] reported structures for Pb_{13}–Pb_{18} and their dipole moments. Large-scale simulations on lead clusters with thousands of atoms using a simple glue-potential were carried by Hendy and Hall.[24–26] In a very recent paper, Kühn[27] investigated Pb_6 at the random phase approximation level and made comparisons with density functional theory. At all levels the octahedral O_h arrangement came out lowest in energy, but with the D_{4h} structure very close by. Density functional theory performed rather well.

Schäfer *et al.*[28] measured the dielectric response of lead clusters at 50 K some years ago. Due to the lack of structural data they have interpreted their results within a perturbation theory model assuming rigid symmetric rotor behavior. Although this procedure gives qualitative insight into the
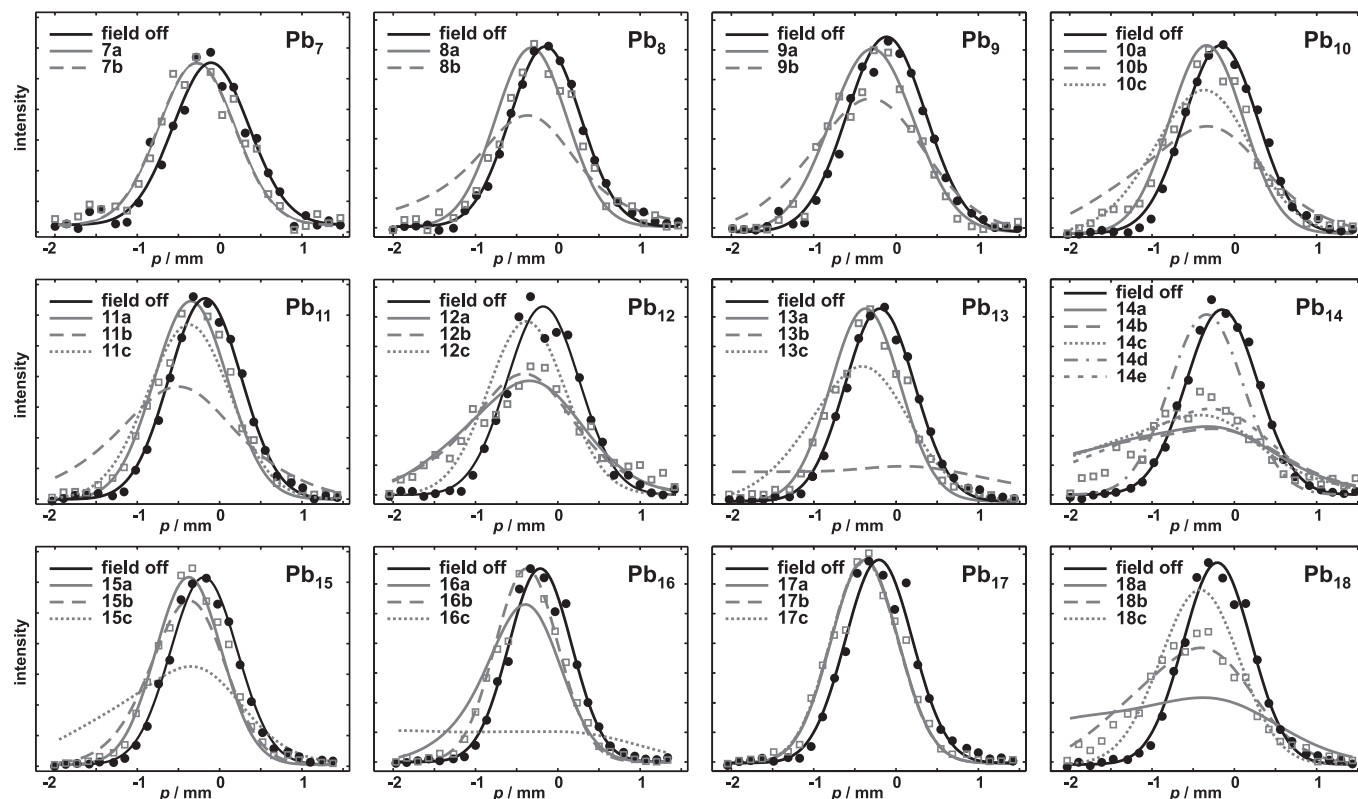
a)goetz@cluster.pc.chemie.tu-darmstadt.de

140, 164313-1

FIG. 1. Beam profiles for Pb$_7$–Pb$_{18}$ without (black circles) and with applied electric field (grey squares). Gaussians are fitted to the data points without applied field as guide to the eye. Solid and dashed grey lines show simulated beam profiles for different isomers. For Pb$_7$ and Pb$_{17}$, simulated beam profiles lie almost on top of each other.

cluster structures, it does not allow their assignment. Additionally, it has turned out to be questionable to treat lead clusters as rigid at 50 K. Therefore, we have repeated these measurements at lower temperature in order to ensure their rigidity and performed an intensive global optimization followed by 2c-DFT structure optimization to consider SO coupling effects. This combination allows the unravelling of equilibrium structures of many neutral lead clusters in the range from 7 to 18 atoms for the first time.

II. EXPERIMENTAL AND COMPUTATIONAL DETAILS

The experimental setup of our molecular beam electric deflection apparatus has been reported in detail elsewhere.[29, 30] Briefly, lead clusters are produced in a pulsed laser vaporization source using helium as carrier gas. The cluster-helium mixture passes a cryogenic nozzle (T_{nozzle} = 20 − 30 K) before it is expanded into a high vacuum chamber where a molecular beam is formed. The molecular beam is shaped by two collimator units before it enters an electric two-wire field unit. A cluster in a quantum state n experiences a deflection d_n

$$d_n = -\frac{A}{mv^2}\frac{\partial E}{\partial z}\frac{\partial \varepsilon_n}{\partial E}, \quad (1)$$

where m and v are the cluster mass and velocity and A is an apparatus constant depending on the electrode geometry. The field gradient $\frac{\partial E}{\partial z}$ is proportional to the applied deflection voltage (28 kV). The Stark effect $\frac{\partial \varepsilon_n}{\partial E}$ is a cluster specific quantity

determining its deflection behavior. Downstream the field the clusters pass a scanning slit plate, are photoionized and subsequently detected using a time-of-flight mass spectrometer. Cluster intensities are measured as a function of the slit position p with and without applied electric field, yielding beam profiles for Pb$_N$ (N = 7–18) as shown in Fig. 1. For a nonpolar cluster, the polarizability α_{exp} can be extracted directly from the beam profile deflection via first order perturbation theory.[28] Experimental polarizabilities are reported for Pb$_N$ (N = 7, 10, 13, 15, 17). For these clusters, no beam broadening is observed, i.e., there is no dipolar contribution to the beam deflection due to a permanent dipole moment.[31]

The configuration space for each considered cluster size is searched using a global optimization approach based on plane-wave self-consistent field (PWscf) DFT using the Quantum Espresso package,[32] coupled with the Lamarckian Birmingham Cluster Genetic Algorithm.[33, 34] For the DFT calculations, 14 electrons for each lead atom are treated explicitly and the remaining 68 electrons are described by an ultrasoft Rabe-Rappe-Kaxiras-Joannopoulos pseudopotential,[35, 36] with a suggested minimum cutoff of 40 Ry. A nonlinear correction was applied and the Perdew-Burke-Ernzerhof (PBE)[37] xc functional is employed within the generalized gradient approximation framework of spin-unrestricted DFT. Within this code, the local optimization of cluster structures is performed in the generation based genetic algorithm with an electronic self-consistency criterion of 10^{-5} eV, and total energy and force convergence considered to be reached when below the threshold values of 10^{-3} eV

and 10^{-2} eV/Å, respectively. Additionally, Methfessel-Paxton smearing is used to improve the efficiency of electronic convergence for metallic states.[38]

Lowest lying isomers are further relaxed at the SR one-component (1c) DFT level using the PBE functional and def2-TZVP basis set with the corresponding effective core potential def2-ecp.[39,40] Here, we use the resolution of the identity (RI-J) and the multipole assisted RI-J method to treat the interelectronic term J.[41,42] Subsequently, harmonic frequency analyses are performed to verify that all structures are true minima, and static polarizabilities are also determined. Static polarizabilities are reported as isotropic polarizabilities α_{iso} obtained from the polarizability tensor. The effect of SO coupling on the polarizability is expected to be small.[43] Finally, 1c-DFT optimized structures are used as starting geometries for 2c-DFT structure optimizations employing def2-TZVP-2c basis sets and def2-ecp-2c effective core potentials.[12] All orbital based electronic structure calculations are carried out using the Turbomole program package.[44] Optimizations at the 2c level lead to a reduced number of local minima (i.e., different starting geometries at 1c level converge to the same minima) and in some cases the dipole moments are changed by some tenths of a Debye.

For a rigid rotor, deflection in an electric field can be simulated by convolution of the undeflected profile with the dipole distribution orientation, which is readily obtained by a molecular dynamics simulation using structural data, dipole moments, and polarizabilities predicted from quantum chemistry.[45] The only free parameter within this simulation is the rotational temperature T_{rot}. Molecular dynamics simulations are therefore carried out for rotational temperatures from 5 to 50 K for all isomers and best agreement with experiment was found for $T_{rot} = 30$ K. The rigidity of the clusters

can be estimated from the harmonic frequency analysis. Since $T_{vib} \approx T_{nozzle}$, vibrational modes below 30 cm^{-1} can influence the rigidity. Some isomers of Pb$_N$ ($N \geq 14$) have modes below 30 cm^{-1} so we have performed experiments for this cluster sizes at $T_{nozzle} = 20$ K. The findings at 30 K could be reproduced, so we conclude the clusters are sufficiently rigid at 30 K.

III. RESULTS AND DISCUSSION

Experimental molecular beam profiles with and without applied electric field are shown in Fig. 1. Low lying structural isomers for Pb$_N$ ($N = 7$–18) from the GA-DFT approach after 2c local optimization are displayed in Fig. 2.

For Pb$_7$, we find the pentagonal bipyramid (PBP) **7a** as global minimum (GM) as previously reported.[20–22] This structure does not have a permanent dipole moment due to symmetry, which is in good agreement with the experimental result. Isomer **7b** is about 0.9 eV higher in energy, but from the experimental point of view cannot be entirely ruled out due to its small permanent dipole moment. The experimental polarizability α_{exp} is 8.9 ± 2.2 Å^3, hence both isomers are within the error of the experiment.

The GM for Pb$_8$ **8a** can be interpreted as a distorted snub disphenoid. The distortion induces a small dipole moment of 0.04 D which fits the experimental data well. Isomer **8b** is analogous to **7a** a PBP with one face capped. Though both structures are quite similar the latter one has a dipole moment of 0.58 D and can therefore be excluded.

The lowest lying isomer for Pb$_9$ (**9a**) consists of two interpenetrating PBP, whereas the bicapped PBP **9b** is already 0.63 eV higher in energy. At 1c-PBE level of theory both isomers have very similar dipole moments of 0.14 and 0.18 D,
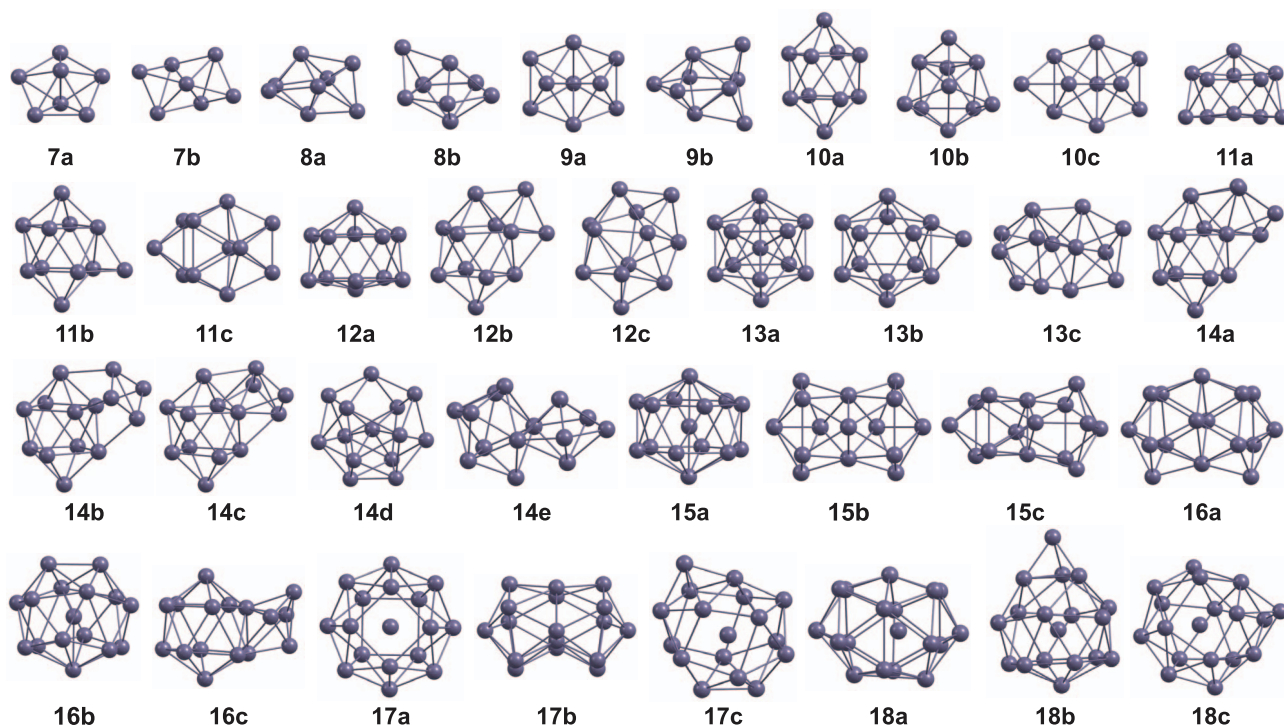

FIG. 2. Locally optimized structures of neutral lead clusters at the 2c-PBE level of theory. Relative energies and symmetries are given in Table I.

TABLE I. Symmetries, relative energies, dipole moments at 2c-PBE level of theory, and isotropic polarizabilities at 1c-PBE level of theory of neutral lead clusters. Corresponding structures are displayed in Fig. 2. χ^2 is the least square measure for a simulated beam profile fit to the experimental data points.

	Symmetry	ΔE (eV)	μ (D)	α_{iso} (Å³)	χ^2
7a	D_{5h}	0.00	0.00	8.06	0.08
7b	C_2	0.89	0.02	8.45	0.08
8a	C_s	0.00	0.04	8.17	0.09
8b	C_s	0.15	0.59	8.54	0.23
9a	C_{2v}	0.00	0.16	8.01	0.07
9b	C_{2v}	0.63	0.44	8.22	0.14
10a	D_{4d}	0.00	0.00	7.95	0.05
10b	C_{3v}	0.06	0.57	7.96	0.24
10c	C_s	0.56	0.38	8.34	0.08
11a	C_{2v}	0.00	0.09	7.99	0.04
11b	C_s	0.12	0.78	8.06	0.44
11c	C_{2v}	0.13	0.28	8.12	0.08
12a	C_{5v}	0.00	0.59	7.90	0.03
12b	C_s	0.38	0.65	8.17	0.04
12c	C_1	0.42	0.27	8.07	0.22
13a	I_h	0.00	0.00	7.93	0.05
13b	C_{3v}	0.38	2.22	7.99	1.14
13c	C_1	0.57	0.52	8.17	0.15
14a	C_1	0.00	1.35	8.26	0.12
14b	C_s	0.04	1.34	8.43	0.13
14c	C_1	0.07	1.27	8.16	0.09
14d	C_s	0.10	0.19	8.07	0.50
14e	C_s	0.32	1.07	8.47	0.07
15a	D_{6d}	0.00	0.00	7.78	0.05
15b	C_{2v}	0.49	0.43	8.24	0.10
15c	C_s	0.53	0.90	8.32	0.55
16a	C_{2v}	0.00	0.59	8.29	0.10
16b	C_{2v}	0.09	0.12	7.82	0.03
16c	C_s	0.17	2.27	8.17	1.37
17a	D_{4d}	0.00	0.00	7.76	0.03
17b	C_{2v}	0.09	0.05	8.02	0.04
17c	C_s	0.48	0.08	7.89	0.04
18a	C_s	0.00	1.59	7.84	0.30
18b	C_{3v}	0.02	0.85	7.92	0.05
18c	C_1	0.05	0.41	7.86	0.14

respectively. This similarity is lifted at the 2c-PBE level of theory (see Table I) and allows the exclusion of **9b** due to its large dipole moment.

The bicapped quadratic antiprism **10a** is the GM for Pb$_{10}$. Although this structure has been reported several times before it was never identified as the GM because the tetracapped trigonal prism **10b** was found to be lower in energy. We confirm this by 1c calculations. However, after 2c structure optimization **10a** is 0.06 eV lower in energy than **10b**. Experimentally, a structure without a dipole moment is expected, which is perfectly met by **10a**. Due to its simulated beam profile the TTP **10b** can be excluded as well as the PBP based structure **10c**. The experimental polarizability α_{exp} is 7.5 ± 1.6 Å³ so the theoretically estimated value lies within the error.

The GM for Pb$_{11}$ is the C_{2v} symmetric structure **11a** which has been reported by other authors.[20,21] It has a small dipole moment of 0.09 D and fits the data well (χ^2 = 0.05). Two further isomers **11b** (based on a bicapped

quadratic antiprism) and **11c** (based on a trigonal prism) have significantly larger dipole moments and do not fit the experimental data as well as **11a**. This still holds if T_{rot} is increased to 50 K in the molecular dynamics simulation.

For Pb$_{12}$, we find a distorted icosahedron as GM, which fits the experimental beam profile very well. Nevertheless, there exists a second isomer **12b** 0.4 eV higher in energy which has not been reported before. It resembles the bicapped tetragonal antiprisms **10a** and **11b** with two triangular faces capped. Its dipole moment of 0.64 D gives rise to a very similar beam profile and hence this isomer cannot be excluded experimentally. A third isomer **12c** slightly higher in energy than **12b** can be ruled out due to its small dipole moment of 0.27 D.

An icosahedron with an atom at the center **13a** is found as GM for Pb$_{13}$ (α_{iso} = 7.93 Å³, α_{exp} = 7.7 ± 1.4 Å³). A capped hollow icosahedron which has also been proposed as the GM structure[20] lies 0.38 eV higher in energy. It can readily be ruled out since this structure has a significant permanent dipole moment while no experimental beam broadening is observed. The next lowest lying isomer **13c** is also unable to explain the experimental findings.

For Pb$_{14}$, four isomers are found within a 0.1 eV energy range and about 20 within 0.5 eV, indicating a shallow potential energy surface (PES). Three of the isomers below 0.1 eV are based on the bicapped quadratic antiprism **10a** exhibiting dipole moments of approximately 1.3 D. Isomer **14d** has a small dipole moment of 0.19 D. None of these isomers are able to describe the experimental data sufficiently. There may be several reasons for this result. Although the GA has been restarted several times, it remains possible that the correct global minimum structure has not been found. Further, due to the shallow PES it seems possible that more than one isomer is present in the molecular beam. Additionally, there exists an isomer 0.32 eV higher in energy which would normally be excluded but fits the data quite well. It is the same structure as found experimentally for Pb$_{14}^+$.[15] An unambiguous attribution of an equilibrium structure for Pb$_{14}$ is not possible based on our data.

A bicapped hexagonal antiprism with an atom in the center **15a** is the predicted GM for Pb$_{15}$. This structure gives rise to a vanishing dipole moment which fits the experimental result well, i.e., no beam broadening is observed (α_{exp} = 7.0 ± 1.2 Å³). The other two local minimum structures found are about 0.5 eV higher in energy than **15a** and their presence in the molecular beam can be ruled out based on their large dipole moments of 0.43 and 0.90 D, respectively.

The GM structure for Pb$_{16}$ is the prolate species **16a**. It has a large dipole moment (0.59 D), in contrast to the experimental finding where no beam broadening is observed. The second lowest lying isomer **16b** (+0.09 eV) is spherical and fits the experimental data very well. Isomer **16c** is an icosahedron with an interpenetrating PBP. It has a large dipole moment and can therefore be ruled out.

The GM structure of Pb$_{17}$ is a highly symmetric D_{4d} structure **17a** which fits the experimental data best. However, two other isomers **17b** and **17c** are about 0.1 and 0.5 eV higher in energy, respectively, but are also in very good agreement with the experiment. Calculated polarizabilities are all within

the error of the experiment ($\alpha_{\text{exp}} = 7.1 \pm 1.2$ Å^3). Therefore, they cannot be ruled out on the basis of our experiment.

As for Pb$_{12}$ and Pb$_{14}$, a significant beam broadening is observed for Pb$_{18}$. Three low lying isomers are located by the GA within an energy range of 0.05 eV. The C_s symmetric isomer **18a** has a dipole moment of 1.59 D yielding a broader beam profile than expected from the experiment even if a higher rotational temperature is assumed. Isomer **18b**, only 0.02 eV higher in energy, fits the experimental beam profile very well. Interestingly, the dipole moment of **18b** is significantly reduced at 2c-PBE level of theory. At SR level of theory none of the isomers would be able to reproduce the experimental result. Isomer **18c** is still very close in energy but its dipole moment of 0.41 D is far too small to fit the observed broadening.

Kelting *et al.*[15] have resolved the structures of most lead cluster anions and cations in the range from 4 to 15 atoms by ion mobility and collision induced dissociation measurements. Cations and anions have the same structure for Pb$_7$ and Pb$_8$, i.e., a PBP and a snub disphenoid, which is also found for the neutral species. Neutral Pb$_9$, Pb$_{11}$, Pb$_{13}$, and Pb$_{15}$ clusters resemble the cationic structures. Pb$_{10}$ favors a bicapped quadratic antiprism, i.e., the same structure as Pb$_{10}^-$ which is also found for the Zintl ion Pb$_{10}^{2-}$ in solution.[46] The situation remains ambiguous for Pb$_{12}$ since neither drift mobility nor beam deflection experiments can make a distinct assignment of the structure, though the distorted icosahedron **12a** is postulated based on both experiments. A hollow icosahedron as found for Pb$_{12}^-$ and Pb$_{12}^{2-}$ can clearly be ruled out.[47] Experimental beam profiles for Pb$_{14}$ can be explained by isomer **14e** which resembles the cationic structure but there is no clear evidence from our data. Seven, eight, and nine-atom lead clusters exhibit the same equilibrium structures as Si, Ge, and Sn (as far as they have been resolved).[45, 48–52] From 10 atoms onwards the structures of lead clusters differ fundamentally from those found for tin, germanium, and silicon. Whereas these elements adopt mainly prolate structures based on a tetracapped trigonal prism, lead prefers spherical structures with denser packing. As outlined above, bicapped quadratic antiprims and pentagonal bipyramids are repetitive motifs in medium sized lead clusters.

IV. CONCLUSION

We have reported molecular beam electric deflection studies and an extensive DFT based global optimization followed by 2c DFT local optimizations for Pb$_N$ ($N = 7$–18). Experimental polarizabilities are in qualitative agreement with calculated values for clusters where no dipolar contribution to the polarizability is expected. Equilibrium geometries can be assigned for most cluster sizes by comparison of measured and modelled beam profiles. Including SO effects is crucial for some cluster sizes, where the relaxation of the geometry leads to significant changes in the dipole moment. Deviations of the growth pattern from silicon, germanium, and tin clusters estimated from previous quantum chemical calculations can be confirmed experimentally for neutral species with more than ten atoms. For some cluster sizes, e.g., Pb$_{17}$, we are not able to clearly determine an equilibrium structure

due to many low lying isomers with similar permanent dipole moments. Since the transition to metallic behavior should be mirrored by the dielectric properties (i.e., vanishing dipole moments and metallic sphere like polarizabilities), we aim to extend this study to over 50 atoms as recently achieved for silicon.[53]

[1]P. Pyykkö, Chem. Rev. **88**, 563 (1988).
[2]J. Desclaux, At. Data Nucl. Data Tables **12**, 311 (1973).
[3]P. Schwerdtfeger, G. A. Heath, M. Dolg, and M. A. Bennett, J. Am. Chem. Soc. **114**, 7518 (1992).
[4]P. Schwerdtfeger, H. Silberbach, and B. Miehlich, J. Chem. Phys. **90**, 762 (1989).
[5]K. K. Das, H. P. Liebermann, R. J. Buenker, and G. Hirsch, J. Chem. Phys. **104**, 6631 (1996).
[6]R. Ahuja, A. Blomqvist, P. Larsson, P. Pyykkö, and P. Zaleski-Ejgierd, Phys. Rev. Lett. **106**, 018301 (2011).
[7]J. R. Anderson and A. V. Gold, Phys. Rev. **139**, A1459 (1965).
[8]T. L. Loucks, Phys. Rev. Lett. **14**, 1072 (1965).
[9]A. Hermann, J. Furthmüller, H. W. Gäggeler, and P. Schwerdtfeger, Phys. Rev. B **82**, 155116 (2010).
[10]K. S. Pitzer, J. Chem. Phys. **63**, 1032 (1975).
[11]P. Schwerdtfeger, Nat. Chem. **5**, 636 (2013).
[12]M. K. Armbruster, W. Klopper, and F. Weigend, Phys. Chem. Chem. Phys. **8**, 4862 (2006).
[13]B. Waldschmidt, M. Turra, and R. Schäfer, Z. Phys. Chem. **221**, 1569 (2007).
[14]A. A. Shvartsburg and M. F. Jarrold, Chem. Phys. Lett. **317**, 615 (2000).
[15]R. Kelting, R. Otterstätter, P. Weis, N. Drebov, R. Ahlrichs, and M. M. Kappes, J. Chem. Phys. **134**, 024311 (2011).
[16]G. Ganteför, M. Gausa, K.-H. Meiwes-Broer, and H. Lutz, Z. Phys. D **12**, 405 (1989).
[17]C. Lüder and K. Meiwes-Broer, Chem. Phys. Lett. **294**, 391 (1998).
[18]V. Senz, T. Fischer, P. Oelßner, J. Tiggesbäumker, J. Stanzel, C. Bostedt, H. Thomas, M. Schöffler, L. Foucar, M. Martins, J. Neville, M. Neeb, T. Möller, W. Wurth, E. Rühl, R. Dörner, H. Schmidt-Böcking, W. Eberhardt, G. Ganteför, R. Treusch, P. Radcliffe, and K.-H. Meiwes-Broer, Phys. Rev. Lett. **102**, 138303 (2009).
[19]K. Balasubramanian and D. Majumdar, J. Chem. Phys. **115**, 8795 (2001).
[20]B. Wang, J. Zhao, X. Chen, D. Shi, and G. Wang, Phys. Rev. A **71**, 033201 (2005).
[21]C. Rajesh and C. Majumder, J. Chem. Phys. **126**, 244704 (2007).
[22]X.-P. Li, W.-C. Lu, Q.-J. Zang, G.-J. Chen, C. Z. Wang, and K. M. Ho, J. Phys. Chem. A **113**, 6217 (2009).
[23]Y.-M. Lei, L.-X. Zhao, X.-J. Feng, M. Zhang, and Y.-H. Luo, J. Mol. Struct.: THEOCHEM **948**, 11 (2010).
[24]S. C. Hendy and B. D. Hall, Phys. Rev. B **64**, 085425 (2001).

[25]S. C. Hendy and J. P. K. Doye, Phys. Rev. B **66**, 235402 (2002).

[26]J. Doye and S. Hendy, Eur. Phys. J. D **22**, 99 (2003).

[27]M. Kühn, J. Chem. Theory Comput. **10**, 623 (2014).

[28]S. Schäfer, S. Heiles, J. A. Becker, and R. Schäfer, J. Chem. Phys. **129**, 044304 (2008).

[29]T. Bachels and R. Schäfer, Rev. Sci. Instrum. **69**, 3794 (1998).

[30]S. Schäfer, M. Mehring, R. Schäfer, and P. Schwerdtfeger, Phys. Rev. A **76**, 052515 (2007).

[31]M. Schnell, C. Herwig, and J. Becker, Z. Phys. Chem. **217**, 1003 (2003).

[32]P. Giannozzi, S. Baroni, M. C. N. Bonini, R. Car, C. Cavazzoni, D. Ceresoli, G. L. Chiarotti, M. Cococcioni, I. Dabo, A. D. Corso, S. de Gironcoli, S. Fabris, G. Fratesi, R. Gebauer, U. Gerstmann, C. Gougoussis, A. Kokalj, M. Lazzeri, L. Martin-Samos, N. Marzari, F. Mauri, R. Mazzarello, S. Paolini, A. Pasquarello, L. Paulatto, C. Sbraccia, S. Scandolo, G. Sclauzero, A. P. Seitsonen, A. Smogunov, P. Umari, and R. M. Wentzcovitch, J. Phys.: Condens. Matter **21**, 395502 (2009).

[33]R. L. Johnston, Dalton Trans. **4193** (2003).

[34]S. Heiles, A. J. Logsdail, R. Schäfer, and R. L. Johnston, Nanoscale **4**, 1109 (2012).

[35]D. Vanderbilt, Phys. Rev. B **32**, 8412 (1985).

[36]A. M. Rappe, K. M. Rabe, E. Kaxiras, and J. D. Joannopoulos, Phys. Rev. B **41**, 1227 (1990).

[37]J. P. Perdew, K. Burke, and M. Ernzerhof, Phys. Rev. Lett. **77**, 3865 (1996).

[38]M. Methfessel and A. T. Paxton, Phys. Rev. B **40**, 3616 (1989).

[39]F. Weigend and R. Ahlrichs, Phys. Chem. Chem. Phys. **7**, 3297 (2005).

[40]B. Metz, H. Stoll, and M. Dolg, J. Chem. Phys. **113**, 2563 (2000).

[41]K. Eichkorn, O. Treutler, H. Ohm, M. Haser, and R. Ahlrichs, Chem. Phys. Lett. **240**, 283 (1995).

[42]M. Sierka, A. Hogekamp, and R. Ahlrichs, J. Chem. Phys. **118**, 9136 (2003).

[43]A. Devarajan, A. Gaenko, and J. Autschbach, J. Chem. Phys. **130**, 194102 (2009).

[44]TURBOMOLE V6.3 2011, a development of University of Karlsruhe and Forschungszentrum Karlsruhe GmbH, 1989–2007, TURBOMOLE GmbH, since 2007; available from http://www.turbomole.com.

[45]S. Heiles, S. Schäfer, and R. Schäfer, J. Chem. Phys. **135**, 034303 (2011).

[46]A. Spiekermann, S. D. Hoffmann, and T. F. Fässler, Angew. Chem., Int. Ed. **45**, 3459 (2006).

[47]L.-F. Cui, X. Huang, L.-M. Wang, J. Li, and L.-S. Wang, J. Phys. Chem. A **110**, 10169 (2006).

[48]S. Schäfer, B. Assadollahzadeh, M. Mehring, P. Schwerdtfeger, and R. Schäfer, J. Phys. Chem. A **112**, 12312 (2008).

[49]B. Assadollahzadeh, S. Schäfer, and P. Schwerdtfeger, J. Comput. Chem. **31**, 929 (2010).

[50]A. Fielicke, J. T. Lyon, M. Haertelt, G. Meijer, P. Claes, J. de Haeck, and P. Lievens, J. Chem. Phys. **131**, 171105 (2009).

[51]M. Haertelt, J. T. Lyon, P. Claes, J. de Haeck, P. Lievens, and A. Fielicke, J. Chem. Phys. **136**, 064301 (2012).

[52]D. A. Götz, S. Heiles, R. L. Johnston, and R. Schäfer, J. Chem. Phys. **136**, 186101 (2012).

[53]D. A. Götz, S. Heiles, and R. Schäfer, Eur. Phys. J. D **66**, 293 (2012).

[54]See http://www.bear.bham.ac.uk/bluebear for a description of the blue-bear HPC facility.